Wake formation behind positively charged spacecraft in flowing tenuous plasmas

E. Engwall
Department of Astronomy and Space Physics, Uppsala University, Uppsala, Sweden and Swedish Institute of Space Physics, Uppsala, Sweden

A. I. Eriksson
Swedish Institute of Space Physics, Uppsala, Sweden

J. Forest
Swedish Institute of Space Physics, Kiruna, Sweden and Artenum Company, Paris, France

(Received 9 February 2006; accepted 3 April 2006; published online 14 June 2006)

Spacecraft in tenuous plasmas become positively charged because of photoelectron emission. If the plasma is supersonically drifting with respect to the spacecraft, a wake forms behind it. When the kinetic energy of the positive ions in the plasma is not sufficient to overcome the electrostatic barrier of the spacecraft potential, they scatter on the potential structure from the spacecraft rather than get absorbed or scattered by the spacecraft body. For tenuous plasmas with Debye lengths much exceeding the spacecraft size, the potential structure extends far from the spacecraft, and consequently in this case the wake is of transverse dimensions much larger than the spacecraft. This enhanced wake formation process is demonstrated by theoretical analysis and computer simulations. Comparison to observations from the Cluster satellites shows good agreement. © *2006 American Institute of Physics*. [DOI: 10.1063/1.2199207]

I. INTRODUCTION

When a spacecraft moves through a plasma at a relative speed exceeding the ion thermal speed in the plasma, a wake will form behind it. Since in the space plasmas where this happens usually $T_i \sim T_e$, so that the spacecraft also moves faster than ion acoustic waves, we refer to this motion as supersonic. Motion supersonic with respect to electrons as well as ions is rare: the typical case is the mesosonic flow, where the spacecraft is supersonic with respect to the ions but subsonic with respect to the electrons. The wake thus becomes negatively charged, due to the thermal motion of the electrons.

Mesosonic spacecraft motion, and hence the occurrence of a negatively charged wake behind the spacecraft, is very common. The prime examples are the ionosphere and solar wind. In the ionosphere, typical spacecraft move at speeds around 7 km/s in a plasma with ion thermal speed on the order of 4 km/s for protons and 0.25 km/s for oxygen. In the solar wind, a flow speed of 400 km/s and proton thermal speed of 40 km/s are typical values. Less obvious regions of mesosonic spacecraft motion are the polar cap and tail lobes of the Earth's magnetosphere. These regions are sometimes thought of as essentially void of plasma, but are often filled with a very tenuous ($\sim$0.1 cm^{-3}) but mesosonic cold plasma outflow from the ionosphere, driven by, e.g., the polar wind or cleft ion fountain.[1–3] Electric field measurements on the Cluster satellites have shown a regular occurrence of wakes in these regions.[4]

The three regions mentioned present three different regimes for wake formation. In the ionosphere, the spacecraft potential with respect to the surrounding plasma, V_{sc}, usually is negative and a few times the electron temperature T_e in magnitude, due to the higher mobility of electrons. This case has been studied for a long time, and a substantial literature has built up over the years. An old, but still very useful, summary was provided by Al'pert *et al.*,[5] with a review of later work given by Hastings.[6] One of the results is that the negative potential structure, from the spacecraft itself as well as from the negatively charged wake, focuses ions into the wake, enhancing the filling-in of the wake.

The solar wind is much more tenuous than the ionosphere (typically 5 cm^{-3}), implying that the electrons randomly collected by the spacecraft give a current much smaller than the photoemission current from the sunlit spacecraft. The result is positive values of V_{sc}, typically on the order of 5–10 V. This is so much lower than the ion flow kinetic energy of typically 1 keV (protons) that the charge of the spacecraft is quite irrelevant for the wake formation, and the elongated wake forming behind the spacecraft has its width determined by the spacecraft dimensions [see Fig. 1(a)]. Much existing work on theory and simulation of wake formation behind ionospheric spacecraft is relevant for this situation as well.

The case of tenuous mesosonic plasma flows in the terrestrial magnetosphere is quite different. In the very tenuous plasmas of the polar cap and tail lobe regions ($\sim$0.1 cm^{-3} or less), the spacecraft potential often goes above 20 V positive, sometimes as high as 50 V or more.[7] Ion flow energies often stay at much lower values, around 10 eV, with temperatures of a few eV.[3] In this case, i.e., when

$$KT_i < \frac{m_i u^2}{2} < eV_{sc}, \tag{1}$$

the ions will scatter on the repulsive potential distribution from the spacecraft. The wake size transverse to the flow can thus be substantially larger than the spacecraft body itself

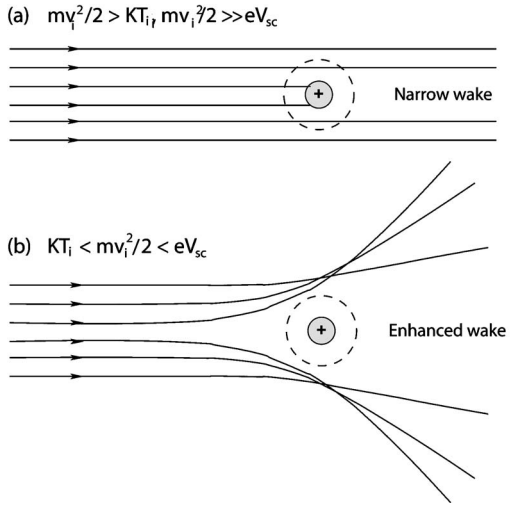

FIG. 1. Sketch of wake formation in mesosonic flows. (a) For ion flow energies much higher than the spacecraft potential, V_{sc}, the wake has the typical transverse size of the spacecraft (narrow wake case). (b) For ion flow energy below V_{sc}, ions will scatter off the positive electrostatic potential from the spacecraft, creating an enhanced wake.

[see Fig. 1(b)]. We call such a wake an enhanced wake.

In contrast to the large literature on wakes behind negatively charged spacecraft, relevant to the ionosphere, very few studies address wake formation behind positive spacecraft, and only one of them concerns the case described by relation (1). The very earliest theoretical studies on spacecraft wake formation treated the case of a wake behind a point charge[8] or line charge[9] in a mesosonic plasma flow in a formalism applicable also for positive charges. As the obstacles in these cases are infinitesimally small, while the calculated wake has a Debye scale width, these studies catch an important feature of the enhanced wake discussed above. However, the assumption of small potentials, $|V_{sc}| \ll m_i u^2/2$, means that they cannot be directly used for quantitative study of wakes in the situation described by relation (1). The same limitation applied to the laboratory study of wakes behind thin cylinders by Hester and Sonin,[10] which included an experiment with positive cylinder potentials, $eV_{sc} \approx 3KT_e \approx 300KT_i \approx m_i u^2/20$. Despite the low potential of the obstacle, they detected an ion void significantly larger than the geometrical size of the obstacle. The elements of an enhanced wake, still in the small potential limit, can also be seen in the results of a simulation of a spherical Langmuir probe in a flowing plasma by Singh and Chagani.[11] The only studies of the case (1) that we are aware of are the simulations of spacecraft in the polar wind flow by Rylina *et al.*[12] and in a cometary coma by Roussel and Berthelier.[13] However, in both cases the plasma has a Debye length much below the spacecraft size, which means that the wake is not significantly enhanced by the electrostatic field around the spacecraft.

In spacecraft applications, the possibility of enhanced wakes was suggested by Bauer *et al.*[14] and Pedersen *et al.*[15] to explain particular features of electric field data from the ISEE (International Sun-Earth Explorer) and GEOS (GEOstationary Scientific Satellite). More recently, Eriksson *et al.*[4] established the presence of enhanced wakes in electric field data from the Cluster satellites. In parallel, we have done the numerical simulations presented in the present paper, using the Cluster data for comparison and verification.

Following this Introduction, we discuss enhanced wake formation in Sec. II, and the results from the computer simulations are presented in Sec. III. In Sec. IV we compare the results from theory and simulations to Cluster data in which the wake is detected.

II. ENHANCED WAKE FORMATION

The condition for enhanced wake formation [see Eq. (1)] ensures that the size of the wake will not be determined directly by the spacecraft's physical structure, but by the equipotential surface, where $\Phi \approx m_i u^2/(2e)$, which few ions can overcome. If we assume vacuum conditions, the characteristic transverse dimension of a spherical spacecraft of radius r at 20 V in a plasma with a flow energy of 5 V will increase from πr^2 to $16\pi r^2$, because the 5 V equipotential is at a distance of 4 r from the center of the spacecraft. This 16-fold increase in obstacle area may seem dramatic, but even more so is the effect on long booms, with which many spacecraft are equipped mainly for measurements of electric fields. Assuming these booms behave like infinite cylinders of radius a in vacuum, except that the potential goes to exactly zero at a distance of $g\lambda_D$, where $g>1$ is a real number, the potential field at a radial distance r from a wire boom at potential V is

$$\Phi(r) = V\frac{\ln(r) - \ln(g\lambda_D)}{\ln(a) - \ln(g\lambda_D)}. \tag{2}$$

From this, we can obtain the radial distance r_b at which $\Phi(r_b)=bV$, where $0<b<1$, as

$$r_b = a^b(g\lambda_D)^{(1-b)}. \tag{3}$$

As an example, let us consider the Cluster wire booms with 88 m tip-to-tip separation and $a=1.1$ mm, a Debye length of 15 m, and an arbitrary but reasonable choice of $g=2$. This gives $r=2.3$ m for the 5 V equipotential around a wire boom at 20 V. The effective size of the booms at right angles to the flow therefore increases from 2.2 mm to 4.6 m, i.e., by three orders of magnitude. This increase depends to some extent on the choice of g, but the effect is certainly significant for all realistic values of g. It is therefore possible that long antennas, which normally are negligible due to their small thickness, can become significant obstacles to the plasma flow in the conditions described by Eq. (1).

How large can the potentials be in the cold, tenuous plasma wake behind the booms? Considering a wake of slablike geometry with thickness $d \ll \lambda_D$, we may assume perfect exclusion of ions and no effect on the electrons. Solving Poisson's equation gives a maximum potential in such a wake of $\Phi_{wake}=(d/\lambda_D)^2 KT_e/e$. For a wake of thickness $d \sim \lambda_D$ or larger, the potential saturates at $\Phi_{wake} \sim KT_e/e$, as further accumulation of electrons is inhibited at larger potentials. The small wake arising behind the booms, for which d is on the order of millimeters, in, for example, the solar wind ($\lambda_D \sim 1$ m), thus cannot give rise to appreciable potentials.

TABLE I. Simulation parameters.

Plasma density, n_0 (cm^{-3})	0.2, 0.4
Electron temperature, KT_e (eV)	1.0, 2.0
Ion temperature, KT_i (eV)	1.0, 2.0
Ion drift kinetic energy, $m_i u^2/2$ (eV)	10
Spacecraft potential, V_{sc} (V)	20, 35
Magnetic field, B (nT)	0

However, significant wake charging will arise in the case of $KT_i < m_i u^2/2 < eV_{sc}$. This wake field may significantly affect the measurements made by a double-probe instrument, as will be discussed in Sec. IV. To provide a more reliable basis for estimates regarding wake formation behind booms and its size, we must turn to simulations. Simulations also provide information on the more geometrically complex wake structure behind the spacecraft body itself.

III. SIMULATIONS OF THE ENHANCED WAKE FORMATION

A. Code and modeling

For modeling of the wake effect behind positively charged spacecraft, we used the open source simulation JAVA-based code package PicUp3D,[16] which implements the particle-in-cell method (PIC)[17] to solve electrostatic spacecraft-plasma interaction problems. PicUp3D is designed for desktop PCs and was run on a dual-processor computer (2×2.40 GHz) with 2 GB RAM. A number of simulations were carried out to examine the wake formation. Results are presented for simulations with two different spacecraft geometries. In the first simulations we modeled only the spacecraft body, while in the other simulations we investigated the effects of long booms, neglecting the effects of the spacecraft body. We used the dimensions of the Cluster spacecraft in our simulations. They are cylindrical with a radius of 1.45 m and a height of 1.5 m. The distance between the boom tips is 88 m. Both the spacecraft surface and a large part of the booms are conductive, so that they are at the same potential (henceforth denoted spacecraft potential, V_{sc}). The last 3 m of the booms closest to the probes consists of different electrical elements at potentials closer to the plasma potential, in order to make the electric field measurements more accurate.[18]

The input parameters for the simulations are chosen to be consistent with high altitude polar wind conditions derived from the POLAR satellite data presented by Su *et al.*[3] as well as with Cluster observations in the polar wind.[19] Table I gives the implemented simulation parameters. With these plasma parameters, the Debye length is in the range $\lambda_D \approx 12-24$ m and the electron plasma frequency $\omega_{pe}/2\pi \approx 4-6$ kHz. The ion flow defines the positive y direction. The integration time steps of all simulations were chosen in such a way that $v_{max}\Delta t < 0.25\Delta r$, where v_{max} is the maximal velocity of any particle, and Δr and Δt the spatial and temporal step sizes, respectively. This ensures that no particle can cross a cell in less than a few time steps. The presented results are averaged over 30 ω_{pe}^{-1} when the solution has reached steady state in order to reduce statistical noise. To speed up the simulations, we used a mass ratio of $m_i/m_e = 100$, while the ion kinetic energy remains unchanged. As will be shown in Sec. III D, this does not change the wake structure close to the spacecraft, but only the filling-in of ions farther downstream.

The magnetic field in magnetospheric regions with cold, tenuous plasmas is normally very low (typically 100 nT) and was neglected in the simulations. This can be justified by the very large Larmor radii (several km) for the two dominant ion species in the polar wind (H^+ and O^+). The electron Larmor radius of a few tens of meters is closer to the scale of the problem. Assuming the electrons to be unmagnetized may lead to overestimation of the electron densities in the wake. Since the flow of electrons is subsonic, this problem should, however, be small.

For simplicity, in none of the cases were photoelectrons included in the simulations. This approximation can be justified by the high potential of the spacecraft (20–35 V), which means that it will recollect most of the emitted photoelectrons, whose typical energies are a few eV.[20] The photoelectrons will thus never build up any appreciable space charge around the spacecraft, and therefore the vacuum potential is a very good approximation.

PicUp3D uses a rectangular grid and Dirichlet boundary conditions, which have a great advantage in their easy implementation, but special care must be taken to ensure that the final results are not influenced substantially. The Dirichlet boundary conditions on the walls of the computational box ($\Phi_b = 0$) can affect the derivation of the potential in the rest of the box, if the walls of the box are too close to the spacecraft. Theoretically, the walls should not be closer to the spacecraft than a few λ_D in order to allow the Debye shielding to decrease the potential to a satisfactorily low level. This assumption was verified numerically for different sizes of computational boxes. On the inner boundary, i.e., at the spacecraft border, the potential is set as an input parameter, and is not calculated self-consistently. The fixed spacecraft potential is of no concern in our case, as the spacecraft potential is related to the plasma density. For Cluster, Pedersen *et al.*[7] extracted a density-potential relation from data. We can thus choose a potential that is consistent with this relation. The rectangular grid can be problematic, since the grid size should be sufficiently small in order to reflect the details of the spacecraft-plasma interactions. On the other hand, the computational box has to be sufficiently large due to the impact on the potential distribution of the Dirichlet boundary conditions. For a detailed description, a large number of computational cells are therefore needed, which leads to long computational times. Thus, the grid size is a compromise between the requirement for a detailed description and reasonable computational times. To be able to resolve finer structures of the booms, we implemented an analytical approximation, namely the *effective potential*, which is discussed in Sec. III C.

TABLE II. Plasma parameters and results from six different simulations. [The lengths of the wakes shown in the table are underestimated, due to the use of artificial mass ratio (see Sec. III D).]

						Length (m)		Width (m)		Height (m)	
Simulation	n_0 (cm^{-3})	V_{sc} (V)	KT_e (eV)	KT_i (eV)	Depth (V)	Φ	n_i	Φ	n_i	Φ	n_i
1	0.20	35	2.0	2.0	−0.37	132	113	97	62	96	55
2	0.20	35	1.0	1.0	−0.39	143	151	84	65	78	57
3	0.20	35	2.0	1.0	−0.60	170	154	111	73	107	65
4	0.20	35	1.0	2.0	−0.23	81	105	62	54	58	49
5	0.40	20	2.0	2.0	−0.32	86	78	68	41	62	36
6	0.40	20	1.0	1.0	−0.35	97	103	57	43	53	39

B. Spacecraft body simulations

To obtain an idea of the wake formation behind the spacecraft body, we ran six reference simulations with different polar wind parameters (see Table II). The drift energy of the ions was 10 eV for all simulations, which is well below the values of the spacecraft potential in Table II. To ensure small effects of the boundary conditions on the final results, the size of the computational box was chosen such that its walls were at least 3 λ_D from the satellite and 1 λ_D from the points where the booms would end if they were included. (The reason for considering the booms, although they are not included in these calculations, was that we wanted to see the signature that would be obtained in a double-probe electric field instrument, which uses such wire booms.) In the downstream direction, the wall was placed at least 10 λ_D away from the satellite to avoid effects of the boundaries on the wake at large distances from the spacecraft.

In all simulations, the grid size was $2.7 \times 2.7 \times 1.35$ m^3, resulting in different numbers of computational cells for different Debye lengths. The spacecraft was modeled as a rectangular box with the same dimensions as the grid, which approximates the cylindrical Cluster spacecraft with a diameter of 2.9 m and a height of 1.5 m fairly well. In general, the average number of particles per cell is eight, which gives a reasonable accuracy. For the first simulation, the number of particles was increased to 100 particles per cell to investigate the effects of particle number on numerical noise. The overall picture remained the same, while the detailed structure of the wake was smoother due to better statistics. Since the computational time increases with increasing numbers of macroparticles, while the noise is proportional to $1/\sqrt{N_{macro}}$,[21] it is costly to reduce the noise. For our purposes, eight particles per cell give sufficient accuracy.

Figure 2 shows results from simulation 1 in Table II. As expected, there is a clearly visible wake in the ion density behind the spacecraft. The dominating potential structure is the decaying potential around the spacecraft, giving essentially spherical equipotentials down to 1 V. Behind the spacecraft a negatively charged wake is formed, reaching a minimum potential of −0.34 V.

The results from all six simulations are shown in Table II, where characteristics of the wake, such as depth (in volts), length, width, and height (in meters), are given. We defined two different criteria to determine the borders of the wake, using the potential (Φ) and the ion density (n_i). For the ion density, the surface where the ion density has decreased to 75% of its background density was used, whereas for the potential we used the equipotential of −0.1 V.

It can clearly be seen that the size of the wake decreases with increasing ion temperature and decreasing electron temperature, which is as expected. A high ion temperature allows the ions to diffuse behind the spacecraft more quickly. Low electron temperatures result in a smaller potential in the wake. Moreover, at low electron temperatures the satellite potential is shielded more efficiently, decreasing the size of the obstacle to the flowing ions. This effect can be seen when comparing the size of the ion wake in simulations 1 and 4. The depths of the wake are relatively large for simulations 5

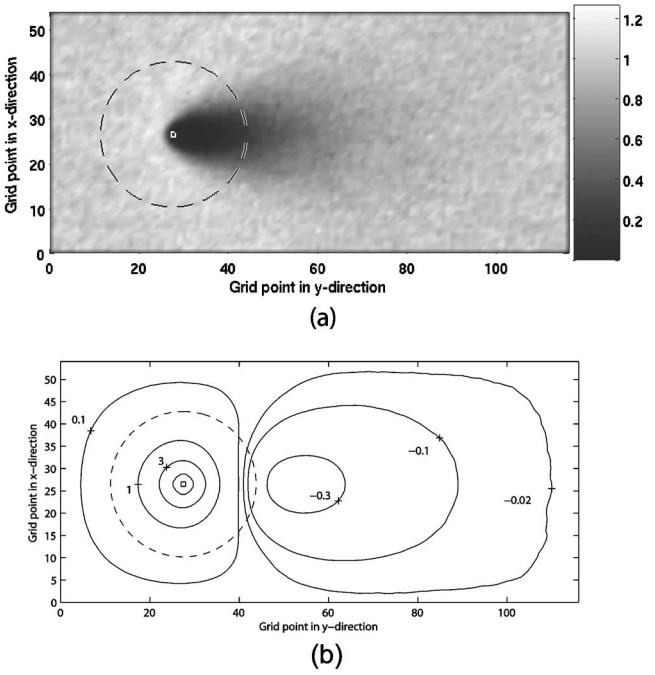

FIG. 2. Averaged normalized density of ions and potential between 20 ω_{pe}^{-1} and 50 ω_{pe}^{-1}. The dashed circles show the location of the Cluster EFW probes throughout a spin period. (The grid spacing is 2.7 m.) (a) Ion density in the *x-y* plane through the spacecraft. (The white square shows the location of the spacecraft.) (b) Potential in the *x-y* plane through the spacecraft (V_{sc} =35 V). The minimum value of the potential in the wake is −0.34 V. Equipotential contours are given at −0.3, −0.1, −0.01, 0.1, 1, 3, 10, and 35 V.

and 6, although the length, width, and height for both the ion and potential wake are comparably small. This is due to the lower spacecraft potential, which will decay faster and thus has less compensating influence where the negative charge accumulation in the wake is strongest.

C. Boom simulations

For the simulations with only booms, we present one specific run with the following plasma parameters: $n_0 = 0.20\ \mathrm{cm}^{-3}$, $KT_e = KT_i = 2.0$ eV, $E_k^i = 10$ eV. The grid size was $4 \times 4 \times 4\ \mathrm{m}^3$ and the number of grid steps in each direction was $N_x = 60$, $N_y = 120$, $N_z = 60$. The boom was assumed to be in the x-y plane at $z = 120$ m at an angle of 45° relative to the flow, which is in the y direction. As PicUp3D includes no explicit provisions for modeling booms, we have instead fixed the potential of 17 discrete grid points, corresponding to a length of 90.5 m, close to the actual length of 88 m. Each grid point on the boom was set to the potential +20 V. (The electrical elements close to the probe described in Sec. III A are thus not represented.) To ensure the validity of a simulation where the booms are represented as discrete grid points, the ion energy should be well below 20 eV, so that no ions can come close to the poorly resolved booms at potential 20 V. In our case, this is not a problem, since the flow energy is 10 eV and the maximum temperature 2 eV.

The ion density and the potential for this simulation are shown in Fig. 3, where it can be seen that the booms indeed play an important role in the formation of an enhanced wake behind the spacecraft. The minimum potential in the wake is −0.80 V, which is substantially larger than for the simulation with spacecraft body (see Sec. III B) with the same plasma parameters.

Solving Poisson's equation on a grid with a spacing of 4 m will result in the potential close to the boom attaining larger values than expected from a wire boom at 20 V, due to the problem of resolving fine structures with a large grid. A few Debye lengths, and hence many grid steps, away from the boom, we may expect the distance dependence on the potential to be realistic, but close to the boom, the simulated potential will decay too slowly with distance. To compensate for this discrepancy, an effective boom potential was calculated by comparison with analytical models. At high potentials close to the boom, the Debye shielding has only small effects and the boom potential can be compared to the vacuum potential of a thin cylinder. The vacuum potential of a thin cylinder at a potential V can be approximated by[22]

$$\Phi(\tilde{x},\tilde{y},\tilde{z}) = \frac{V}{2\ln\left(\frac{l}{a}\right)} \ln\left(\frac{d-\tilde{x}+r_1}{-d-\tilde{x}+r_2}\right), \tag{4}$$

where l is the length of the cylinder, which is aligned with the $\tilde{x}$ axis and centered on the origin, a is its radius, $d = l/2$, $r_1 = \sqrt{(\tilde{x}-d)^2+\tilde{y}^2+\tilde{z}^2}$, and $r_2 = \sqrt{(\tilde{x}+d)^2+\tilde{y}^2+\tilde{z}^2}$. We now look for a value of V in this expression that results in a potential approximating the simulation result around 10 V and a few volts below, as this should be the most sensitive region for the dynamics of the ions whose drift energy is 10 eV. In Fig. 4, the simulated potential (dashed line with circles) is plotted together with the results of the analytical model for a thin boom ($a = 1.1$ mm) potential of 35 V (solid line), as a function of radial distance from the midpoint of the boom. It can be seen that this indeed approximates the simulated potential field around and below 10 V, and we may thus assume that the potential of 20 V applied to the point cluster simulating the booms corresponds to an actual potential as high as 35 V for a real wire boom.

Further away from the boom, Eq. (4) does not give the correct picture, because of the Debye shielding in the plasma. Therefore, at large distances from the boom, it is adequate to compare the simulated boom potential to that of a Debye-shielded infinite cylinder at potential V,

$$\Phi(r) = V \frac{K_0\left(\frac{r\sqrt{2}}{\lambda_D}\right)}{K_0\left(\frac{a\sqrt{2}}{\lambda_D}\right)}, \tag{5}$$

where K_0 is a modified Bessel function of the second kind. The Debye-shielded potential is plotted in Fig. 4 (dashed line) with $a = 1.1$ mm and $V = 35$ V. As expected, the simulated potential and the shielded cylinder approach each other far from the boom. Closer to the boom, the Debye shielding expression (5) breaks down due to violation of the assumption $e\Phi \ll KT_e$ inherent in the linear Debye shielding law. The influence of the wake on the potential can clearly be seen in the difference in the upstream and downstream directions in the simulation data.

To verify the validity of the effective potential, we used two simulations with the spacecraft body for the same plasma parameters but different dimensions ($4 \times 4 \times 4\ \mathrm{m}^3$ and $2.7 \times 2.7 \times 1.35\ \mathrm{m}^3$). In the first simulation, the spacecraft is at 20 V. Using the concept of effective potential, we can expect this to correspond to a potential of $\sqrt[3]{4 \times 4 \times 4/(2.7 \times 2.7 \times 1.35)} \times 20\ \mathrm{V} \approx 37\ \mathrm{V}$ for a spacecraft with dimensions $2.7 \times 2.7 \times 1.35\ \mathrm{m}^3$, assuming scaling of the potential as $1/r$. In the second simulation, the spacecraft potential was set to 35 V. The two simulations give essentially the same potential pattern from a few meters outside the spacecraft, which confirms that the use of effective potentials is acceptable.

D. Accuracy of the simulations

Before comparing the simulation results to spacecraft data, the accuracy of the simulations should be discussed. In terms of basic modeling, two potentially important factors not included in the simulations are the magnetization of electrons (see Sec. III A) and the emission and exchange of photoelectrons by different electrical elements on the spacecraft. It is, for example, possible that the wake is filled to a large extent by photoelectrons emitted from the probes (as noted in Sec. III A, photoelectrons from the spacecraft can never contribute much to the electron density due to the high spacecraft potential), rather than by natural plasma electrons. However, the photoelectron temperature is on the order of a few eV, close to the temperature of the ambient plasma electrons. Therefore, the charge in a wake filled with photoelec-

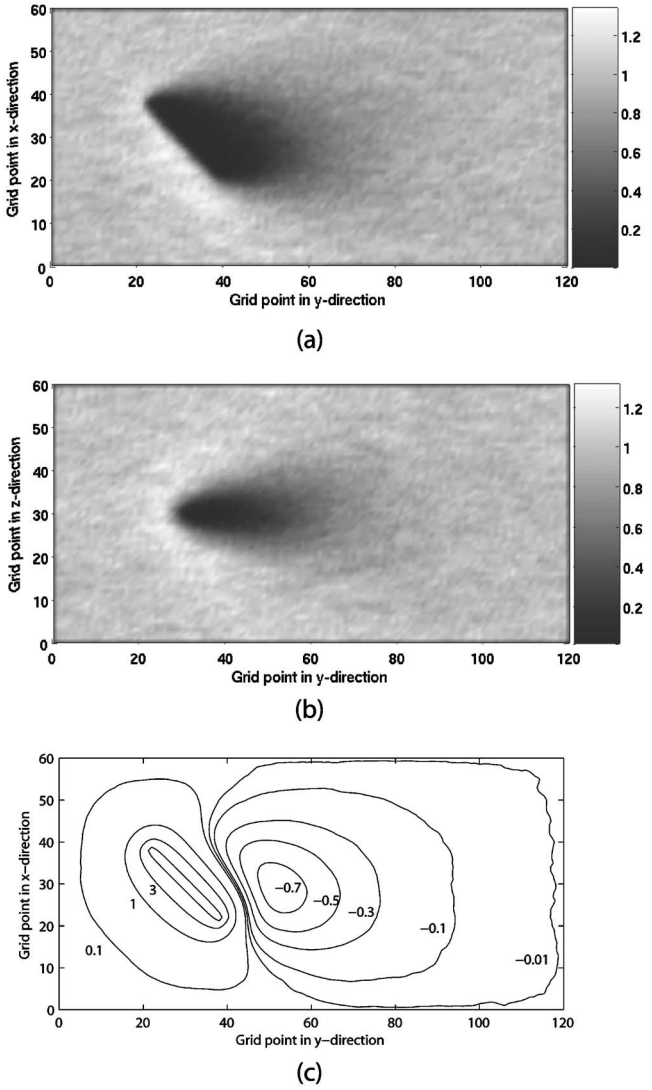

FIG. 3. Averaged results from the boom simulation between 30 ω_{pe}^{-1} and 60 ω_{pe}^{-1}. (The grid spacing is 4 m.) (a) Ion density in the *x*-*y* plane through the boom. (b) Ion density in the *y*-*z* plane through the boom. (c) Potential in the *x*-*y* plane cutting the boom. The minimum value of the potential in the wake is −0.80 V. Equipotential contours are given at −0.7, −0.5, −0.3, −0.1, −0.01, 0.1, 1, 5, and 10 V.

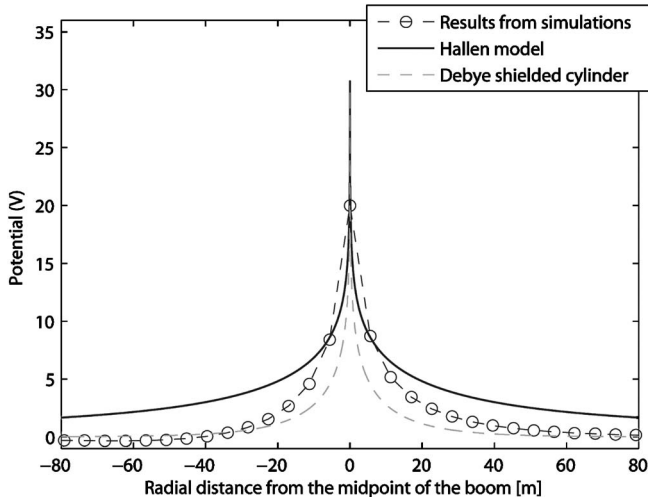

FIG. 4. Comparison between the potential obtained from the simulation (dashed blue line) and analytical models. The red line corresponds to an infinite Debye-shielded cylinder and the black line to the model presented by Hallén (Ref. 22). The horizontal axis gives the radial distance from the center of the boom in the boom-flow plane [r in Fig. 7(b)].

trons should not be very different from the resulting charge in the simulations. Numerical problems that might influence the final results are the unphysical mass ratio, the Dirichlet boundary conditions, and the modeling of the wire booms as discrete grid points.

1. Mass ratio

Using an artificial mass ratio between ions and electrons in the PIC simulations will not significantly influence the wake close to the spacecraft, since the wake potential is small relative to the spacecraft potential distribution. The orbit of a charged particle in any central field is determined completely by its kinetic energy per charge,[23] in analogy with how the Keppler motion in a central gravitational field depends only on kinetic energy per mass, i.e., velocity squared. Deflection in such a potential is therefore accurately represented in a simulation where the kinetic energy is correctly represented, irrespective of the mass actually used. The potential around the spacecraft body can be well approximated as radially symmetric. For the potential around the finite booms, there is no perfect plane of symmetry, but at least for Debye lengths well below the boom length, radial symmetry should be a good approximation in the central part of the boom.

Therefore, we expect the artificial mass ratio to have impact mainly on the filling-in of the wake at large distances from the spacecraft, where the space charge in the wake will dominate the potential, and only if the potential reaches values on the order of the ion temperature. The effect of the mass ratio has been examined by performing simulations 1 to 4 for the spacecraft body with both real ($m_i/m_e=1836$) and artificial ($m_i/m_e=100$) mass ratios. The length of the wake is in average 45% longer for the real mass ratio. However, as expected, the wake structure close to the spacecraft is only marginally affected. This is evident when we examine the simulated signature of a double-probe instrument (see Sec. IV B). The dependence of wake length on mass ratio implies that, for equal flow energies, a wake in an oxygen-dominated plasma will be longer than in a hydrogen-dominated plasma. However, we should also note that at the same flow velocity, oxygen ions are 16 times as energetic as protons, meaning that relation 1 often is not satisfied and thus does not contribute to the wake formation. In the high-altitude polar wind, where many enhanced wakes are observed, the plasma is dominated by protons.[3]

2. Dirichlet conditions

The Dirichlet conditions of the PicUp3D code at the boundaries of the computational box (see Sec. III A) affect the potential close to the boundaries. In the presented simulations, the box was chosen to be sufficiently large to achieve a good overall picture. The potential deep inside the wake is then only marginally affected. As can be seen in Figs. 2(a)

and 3(b), the ion density is not significantly influenced by the Dirichlet conditions, due to the ion energy being high compared to the wake potentials. In a sense, the ions just scatter off the vacuum field of the spacecraft or booms. To verify that the Dirichlet conditions do not constitute a significant error source, we have performed test simulations with 50% larger computational boxes showing that only the potential structures close to the boundaries are affected in the presented simulations.

3. Wire booms

Numerical modeling of 88 m wire booms with a radius of a few millimeters is a computational challenge. We have modeled the booms as a cluster of discrete grid points and compared the potential around the boom to results from analytical models to be able to estimate an *effective potential* for the booms. As described in the previous section, the validity of this effective potential was confirmed for the spacecraft body. For the booms, the method could be verified by comparison to adaptive-grid codes.

IV. COMPARISON TO DATA FROM THE CLUSTER SPACECRAFT

A. Cluster data

The Cluster mission is designed for four-point measurements in key regions of the terrestrial magnetosphere and its adjacent environment in the solar wind, in particular boundary layers such as the bow shock and the magnetopause.[24] Thanks to their polar orbits with perigee at 4 R_E and apogee at 19.6 R_E, the Cluster satellites sample a broad range of plasma regions, from the cold, dense plasma sphere to the hot, tenuous plasma sheet. The four spacecraft were designed with identical payloads, each carrying complete instrumentation for the study of particles and fields. For electric field measurements, Cluster includes two instruments using different techniques. The Electric Fields and Waves instrument (EFW) employs the well-known technique of measuring the voltage between spherical electrostatic probes at the ends of wire booms in the spacecraft spin plane.[18] The technique allows sampling at essentially unlimited frequencies, and can operate under widely varying plasma conditions, although great care is needed in the instrument design in order to minimize electrostatic disturbances from the spacecraft and the probe supports. EFW has two pairs of spherical probes (8 cm in diameter) separated by 88 m wire booms (2.2 mm diameter). In addition to the electric field, EFW provides a measurement of the spacecraft potential with respect to the ambient plasma, V_{sc}. The spin frequency of the satellites is 4 s.

The Electron Drift Instrument (EDI) uses a completely different technique,[25] relying on observing the $\boldsymbol{E}\times\boldsymbol{B}$ drift of electron beams emitted from the spacecraft and returned by the ambient magnetic field, which thus has to be sufficiently strong for the method to work. Using electrons in the keV range, this technique is quite immune to asymmetric electrostatic potentials on the order of a few volts arising close to the spacecraft.

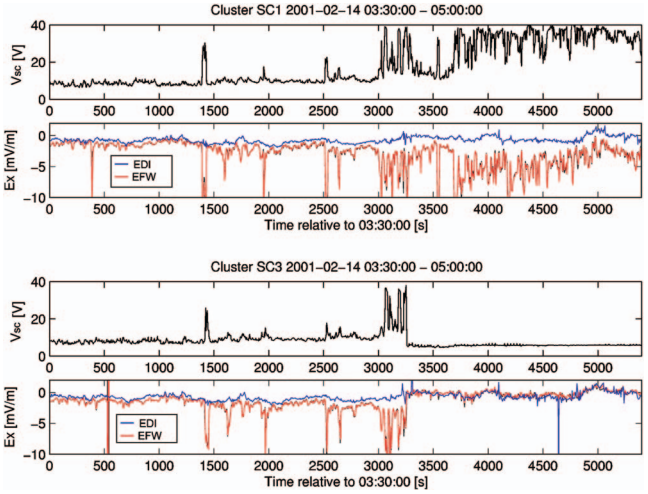

FIG. 5. (Color) EFW and EDI electric field data from SC1 (top two panels) and SC3 (lower two). For each spacecraft, the top panel shows the spacecraft potential V_{sc}, while the lower panel displays the EDI (dashed line) and EFW (solid line) estimates of the sunward component of the electric field. The difference between the two electric field instruments increases when V_{sc} is high. The jump in V_{sc} for SC3 after 3250 s is due to the activation of ASPOC. Large discrepancies between the EDI and EFW electric field estimates can be seen from around 04:20. For SC1, they continue throughout the interval, while they almost disappear from the SC3 data when ASPOC is activated.

We obtained evidence of the enhanced wake mechanism in Cluster data by studying the wake-induced field variations as a function of spacecraft potential. Figure 5 presents data studied in more detail by Eriksson *et al.*[4] In the two upper panels, it can be seen that the data from the EDI and the EFW instruments differ substantially when the spacecraft potential is high. The dependence on spacecraft potential is evident during periods when the artificial potential control instrument, ASPOC,[26] is operating. By emitting a current, typically around 10 μA, of keV ions in a direction normal to the spin plane, ASPOC stabilizes the spacecraft potential at around 7 V. When ASPOC is not operating, V_{sc} reaches values up to +40 V in order to neutralize the photoelectron current emitted by the spacecraft. Figure 5 shows data from two of the Cluster satellites, spacecraft 1 (henceforth denoted SC1) in the top two panels and SC3 in the lower two. At the time in question, Cluster was above the northern polar cap at (−2.5, 1.4, 4.9) R_E in GSE coordinates (GSE X points toward the Sun and GSE Z toward the ecliptic north pole). On SC3, ASPOC was activated at around 3250 s into the plot, resulting in the immediate and clearly visible stabilization of V_{sc}. In the SC1 data, EFW and EDI are seen to differ by up to 10 mV/m after 3000 s, and onwards. Only E_X is shown, as almost all of the wake-induced field was found in this component in this case. The same EDI-EFW discrepancy was seen initially in the SC3 data, but when ASPOC was activated, the difference was greatly diminished. This is exactly the behavior we would expect from a wake created by the spacecraft potential distribution, as discussed above: i.e., when V_{sc} decreases, so does the size of the wake and, hence, the perturbation it causes to the potential field around the spacecraft. The clear relation between the natural variations in spacecraft potential and the wake-induced field that can be

seen in the SC1 data indicates that V_{sc} is the controlling parameter, regardless of whether it is regulated by the plasma environment or by ASPOC.

Since the ions emitted by ASPOC are highly energetic, they will travel far from the spacecraft, and the asymmetries introduced in the sheath around the spacecraft because of the ion beam do not substantially affect the EFW measurements. A complete analysis of the effects on EFW due to the operation of ASPOC is beyond the scope of this paper, but we point out that the effects other than the stabilization of the spacecraft potential are relatively small. ASPOC is therefore quite different from the PSI (Plasma Source Instrument) on the POLAR satellite, which creates a cloud of cold plasma around the spacecraft and has been reported to introduce spurious signals in electric field measurements.[27,28]

From the theoretical estimates of the size of the wake potential in Sec. II, we can obtain an upper limit for the magnitude of the effect on the EFW double-probe instrument. Assuming that the potential in the wake is maximal (i.e., on the order of KT_e) and that one probe experiences the full wake potential and the other nothing, there would be a wake-induced electric field signal in the double-probe instrument of the order of $KT_e/(2le)$, where $2l$ is the separation between the two probes, i.e., 88 m for EFW. In the polar wind, with KT_e values on the order of a few eV, we find that wake-induced fields up to a few tens of mV/m could indeed be possible, which is actually observed. To obtain more precise estimates of the wake effect on the double-probe instrument, we use the results from the two types of simulations.

B. Comparison to spacecraft body simulations

First, we examined the effect of the spacecraft body. To obtain an estimate of the influence of the wake on the double-probe instrument, we considered the potential difference between two points on opposite sides of the spacecraft separated by the boom length of 88 m. An advantage of only considering the wake effect of the spacecraft body is that we do not have to fix the angle of the booms relative to the flow. We can therefore plot the potential difference between the probes as a function of the angle of the virtual booms relative to the flow. Figure 6(a) shows such plots for the first four simulations in Table II together with EFW data from one spin.

As expected, the plot in Fig. 6(a) is periodic with maximum differences at 0° and 180° relative to the flow, and minimum differences at 90° and 270°. It can be seen that the agreement between the EFW data and the results from simulations is good in this case. Comparison between the simulation and data plots provides clarification of the previously unexplained signature in the satellite data. From the simulation it can be seen that an inflection point arises when the probes change the roles of being the closest or farthest away from the wake. The magnitude of the potential difference is also consistent with Cluster measurements in tenuous plasmas, where spurious electric fields on the order of 5 -10 mV/m can be detected.[4] The shape of the signatures from the double-probe instrument is dependent on the plasma parameters. Thus, the wake-field signatures could possibly be used to derive the properties of the plasma. Figure 6(b) shows the signature from a double-probe instrument for simulations with both real and unphysical mass ratios. It can clearly be seen that the double-probe instrument signature is only marginally affected by the choice of mass ratio, as expected (see Sec. III D).

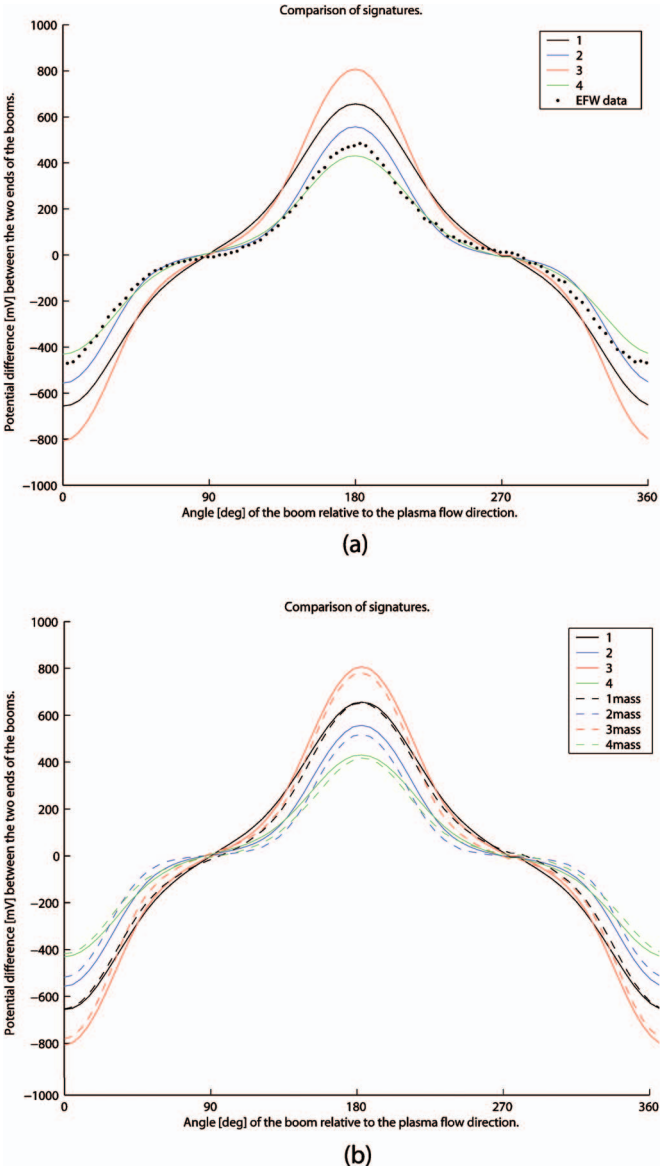

FIG. 6. (a) (Color) Potential difference between the probes at different angles of the boom relative to the flow for the four first simulations (solid lines) together with electric field measurements (dotted lines) from the pair of probes 34 of the EFW instrument on SC3 during one spin period (4 s) at 2002-02-13 01:48:06-10. (b) Simulations 1-4 with real (dashed lines) and unphysical (solid lines) mass ratio. The signatures are only marginally effected by the unphysical mass ratio.

C. Comparison to boom simulations

As for the spacecraft, we will now use the boom simulations to quantify the effect of the boom wake field on the double-probe electric field instrument. In Fig. 7(a), the difference in potential between two probes at the same distance from the opposite ends of the wire boom is plotted as a function of the distance from the boom ends. The maximum

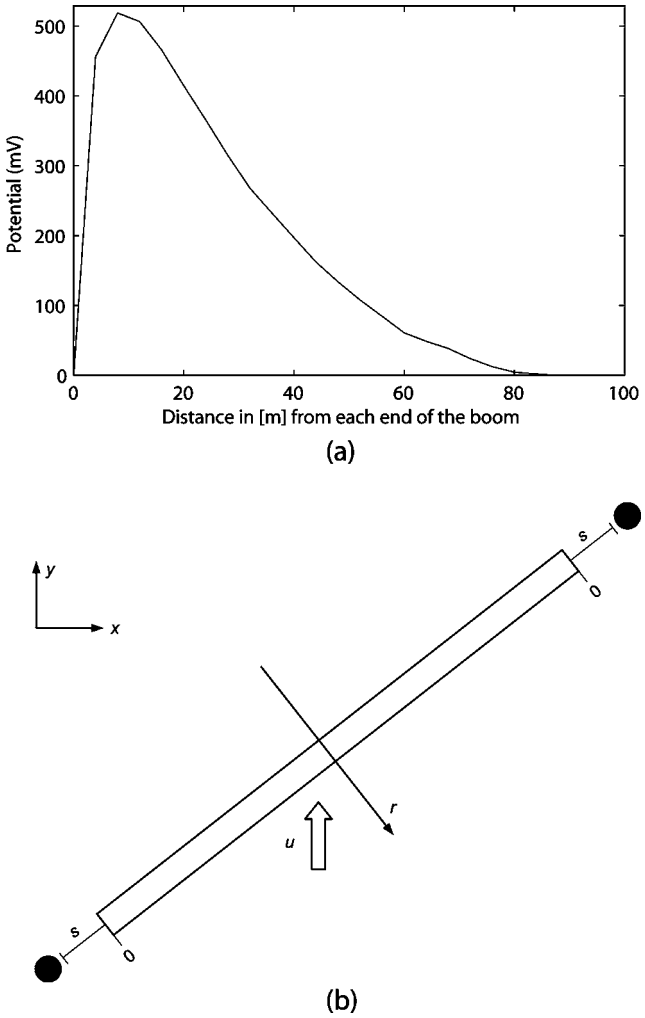

FIG. 7. (a) Difference in potential between the ends of the boom inferred from the simulation with booms only. The maximum potential difference is 520 mV. (b) Schematic picture of the boom explaining the horizontal axis of (a): s is the distance from the boom end to the probe. (The coordinate r is the radial distance from the midpoint of the boom used in Fig. 4.)

potential difference is approximately 520 mV. As expected, the difference is zero far away from the booms, where there is an unperturbed plasma, and also at the boom tips, which are at satellite potential. As mentioned in Sec. III A, the Cluster EFW probes are 3 m outside the part of the wire booms that are at spacecraft potential. One grid spacing distance (4 m) away from the boom on each side, which is close to the relevant 3 m, the observed potential difference is 460 mV. Dividing this by 90.5 m, we find that EFW could be expected to show an apparent electric field of 5 mV/m due to the boom wake. However, since the virtual probes in this case are so close to the boom potential, they will be affected by the boom potential, and the 5 mV/m should be regarded as an order of magnitude estimate of the apparent electric field. Another limitation of the boom simulation in comparison to the setup of the Cluster satellites is that we have only modeled one of the boom pairs. The wake effect should be even greater with two crossed booms. Comparing the resulting potential difference from the boom simulation to the spacecraft body simulation at 45° with the same plasma parameters (simulation 1), we see that the 460 mV from the boom simulation is substantially larger than from the spacecraft body, which results in a potential difference of 250 mV.

From comparing the potential patterns in Figs. 2(b) and 3(c), we can immediately see that the dominating source for the potential at the probes is the booms, not the spacecraft body. Also, the wake is much larger in the boom simulation than in the spacecraft simulation. When the spacecraft and booms spin, the wake and its associated potential should change, and hence also the wake signal detected by a double-probe instrument. So can it be reasonable to assume that the spin signature for a double-probe instrument, derived from the simulation without booms and shown in Fig. 6, should represent reality?

If we first consider the question of spin variation of the wake itself, we can note that this could be a problem mainly if the flow direction is in the spin plane, so that the obstacle, i.e., the $\Phi=\frac{1}{2}m_i u^2/e$ equipotential, as seen from the direction of the approaching ions, would vary significantly in size and shape: small and circular when the boom is aligned to the flow, much elongated when the angle of attack is oblique. However, as the real Cluster spacecraft have two orthogonal pairs of wire booms, the obstacle seen by the approaching ions will always be elongated, regardless of spin phase. Therefore, we do not expect the nonvariation of the wake with spin phase to be a significant error source in the spacecraft body simulations.

But could not the shape of the spin signature presented in Fig. 6 be influenced by the local potential close to the probe, which is certainly drastically changed when the booms are included? Close to the booms, the charge density is low, and the potential is mainly the vacuum potential, which is symmetric between the two probes and hence does not affect the voltage measured between them. Significant charge densities, distributed over regions of size on the order of λ_D so that they can give rise to any appreciable potentials, are found mainly in the wake, as is easily seen in Figs. 2(b) and 3(c). The "distant" source of the wake is therefore the more important one for the potential difference detected at the probes. As the presence of this source, albeit not its magnitude, is similar in the boom and spacecraft body simulations, we expect the shape of the spin variation shown in Fig. 6 to be approximately the same also in the case of booms only. Nevertheless, this remains a point that should be clarified in future simulations (see Sec. V).

As for the magnitude of the wake effect, this is clearly larger for the boom simulations than for the case of the spacecraft body. This is clear from the minimum potentials observed in Figs. 2(b) and 3(c) as well as from the comparison of the values at 45° that we discussed above. It is thus reasonable to expect the spacecraft body simulations to underestimate the magnitude of the wake effect on double-probe measurements. The good agreement between simulated and observed spin signatures in Fig. 6(a) should then imply that some of the input parameters for the simulation do not reflect the real situation. The most likely error source would be an overestimate of the electron temperature T_e, for which we lack any experimental data and have only assumed

a value on the order of T_i. Other parameters (n_e, T_i, v_i, V_{sc}) all have error sources associated, but their values are much better founded on measurements either from Cluster[19] or other spacecraft in the same region.[3]

V. CONCLUSIONS

We have studied the wake formation behind positively charged spacecraft in cold, flowing, tenuous plasmas. Theoretical estimates together with simulations have given new information on the size of the wake. Data from the electric field instruments on board the Cluster spacecraft have provided experimental evidence of the wake formation in cold, flowing, tenuous plasmas. The wake will be enhanced in these regions, which is explained by the fact that $KT_i < m_i u^2 < eV_{sc}$. It was indeed found that the satellite potential, V_{sc}, controls the size of the wake, which is especially evident when the potential is reduced by the ASPOC instrument. More detailed analysis of the experimental data has been given by Eriksson *et al.*[4] A simulation of the wake field detected by the Cluster electric field instrument EFW resulted in 5–10 mV/m, which is close to observed magnitudes, and the variation on spacecraft spin was well represented. This was obtained from simulations of the spacecraft body and the booms separately. The combined effect of both should be somewhat higher.

In future work, an adaptive-grid code with the ability to resolve finer structures, such as wire booms, should be used. Such a code would also allow us to simulate any angle between the flow and the booms, making it possible to obtain more reliable spin signatures. It would also be rewarding to model a more realistic spacecraft geometry with both body and booms, including important electric elements close to the probes. The code should not be implemented only with Dirichlet conditions, but with more flexible boundary conditions. For this kind of problem, Neumann conditions on all sides except the inflowing boundary are better suited. An example of such a code is the Spacecraft Plasma Interaction Software, SPIS (Roussel *et al.*, in *Proceedings of the 9th Spacecraft Charging Technology Conference*, Tsukuba, Japan, 2005). In spite of these desirable improvements, the present study has shown that a simple and open source simulation code package can be run on a common desktop PC to give quantitative results for this kind of spacecraft-plasma interaction problem. The main conclusions that can be drawn from this work are as follows.

1. The qualitative hypothesis of an electrostatic wake with dimensions determined by the spacecraft potential field forming in situations with $KT_i < m_i u^2 < eV_{sc}$ was quantitatively verified by simulations.
2. Both the spacecraft body and the wire booms create large enhanced wakes in these situations. The effective size of the wire booms transverse to the flow can be increased from millimeters to meters.
3. The size of the wake scales with the plasma parameters, of which the two most important features are:
   (a) low ion temperature causes larger ion wake, and
   (b) high electron temperature leads to more negative potential in the wake.
4. The signatures from the electric field data agree well with the simulations, and their shape and magnitude depend on plasma parameters. It is therefore possible in principle to derive plasma parameters from wake observations in electric field data. The first application of this was presented by Engwall *et al.*[19]

[1] A. W. Yau and M. André, Space Sci. Rev. **80**, 1 (1997).
[2] T. E. Moore, C. R. Chappell, M. O. Chandler, P. D. Craven, B. L. Giles, C. J. Pollock, J. L. Burch, D. T. Young, J. H. Waite Jr., J. E. Nordholt, M. F. Thomsen, D. J. McComas, J. J. Berthelier, W. S. Williamson, R. Robson, and F. S. Mozer, Science **277**, 349 (1997).
[3] Y.-J. Su, J. L. Horwitz, T. E. Moore, B. L. Giles, M. O. Chandler, P. D. Craven, M. Hirahara, and C. J. Pollock, J. Geophys. Res. **103**, 29305 (1998).
[4] A. I. Eriksson, M. André, B. Klecker, H. Laakso, P.-A. Lindqvist, F. Mozer, G. Paschmann, A. Pedersen, J. Quinn, R. Torbert, K. Torkar, and H. Vaith, Ann. Geophys. **24**, 275 (2006).
[5] Y. L. Al'pert, A. V. Gurevich, and L. P. Pitaevskii, *Space Physics with Artificial Satellites* (Consultants Bureau, New York, 1965).
[6] D. E. Hastings, J. Geophys. Res. **100**, 14457 (1995).
[7] A. Pedersen, P. Décréau, P. Escoubet, G. Gustafsson, H. Laakso, P.-A. Lindqvist, B. Lybekk, F. Mozer, and A. Vaivads, Ann. Geophys. **19**, 1483 (2001).
[8] L. Kraus and K. W. Watson, Phys. Fluids **1**, 480 (1958).
[9] S. Rand, Phys. Fluids **3**, 588 (1960).
[10] S. D. Hester and A. A. Sonin, Phys. Fluids **13**, 641 (1960).
[11] N. Singh and V. S. Chagani, J. Geophys. Res. **102**, 195 (1997).
[12] I. V. Rylina, L. V. Zynin, S. A. Grigoriev, and M. V. Veselov, Cosmic Res. **40**, 367 (2002).
[13] J.-F. Roussel and J.-J. Berthelier, J. Geophys. Res. **109**, A01104 (2004).
[14] O. H. Bauer, R. Grard, G. Haerendel, and A. Pedersen, Proceedings of the 17th ESLAB Symposium on "*Spacecraft/Plasma Interactions and their Influence on Field and Particle Measurements*" (ESA, Noordwijk, 1983), p. 51.
[15] A. Pedersen, C. A. Cattell, C.-G. Fälthammar, V. Formisano, P.-A. Lindqvist, F. Mozer, and R. Torbert, Space Sci. Rev. **37**, 269 (1984).
[16] J. Forest, A. Hilgers, B. Thiébault, L. Eliasson, J.-J. Berthelier, and H. De Feraudy, IEEE Trans. Plasma Sci. (submitted).
[17] C. K. Birdsall and A. B. Langdon, *Plasma Physics via Computer Simulations* (Adam Hilger, Bristol, 1991).
[18] A. Pedersen, F. Mozer, and G. Gustafsson, in "Measurement Techniques in Space Plasmas — Fields" (AGU, Washington, D.C., 1998).
[19] E. Engwall, A. I. Eriksson, M. André, I. Dandouras, G. Paschmann, J. Quinn, and K. Torkar, Geophys. Res. Lett. **33**, L06110 (2006).
[20] A. Pedersen, Ann. Geophys. **13**, 118 (1995).
[21] R. D. Sydora, Lect. Notes Phys. **615**, 109 (2003).
[22] E. Hallén, *Electromagnetic Theory* (Chapman & Hall, London, 1962).
[23] L. D. Landau and E. M. Lifshitz, *Course of Theoretical Physics, Vol. 1: Mechanics*, 3rd ed. (Pergamon Press, New York, 1976).
[24] C. P. Escoubet, M. Fehringer, and M. Goldstein, Ann. Geophys. **19**, 1197 (2001).
[25] G. Paschmann, C. E. McLlwain, J. M. Quinn, R. B. Torbert, and E. C. Whipple, in "Measurement Techniques in Space Plasmas — Fields" (AGU, Washington D.C., 1998).
[26] K. Torkar, W. Riedler, C. P. Escoubet, M. Fehringer, R. Schmidt, R. J. L. Grard, H. Arends, F. Rüdenauer, W. Steiger, B. T. Narheim, K. Svenes, R. Torbert, M. André, A. Fazakerley, R. Goldstein, R. C. Olsen, A. Pedersen, E. Whipple, and H. Zhao, Ann. Geophys. **19**, 1289 (2001).
[27] R. H. Comfort, T. E. Moore, P. D. Craven, C. J. Pollock, F. S. Mozer, and W. T. Williamson, J. Spacecr. Rockets **35**, 845 (1998).
[28] N. Singh, W. C. Leung, T. E. Moore, and P. D. Craven, J. Geophys. Res. **106**, 19179 (2001).